First-principles study of electronic structures and nonlinear optical properties of $AMoO_3(IO_3)$ (A = Li, Rb and Cs) crystals

2010 J. Phys.: Condens. Matter 22 155801

(http://iopscience.iop.org/0953-8984/22/15/155801)

J. Phys.: Condens. Matter **22** (2010) 155801 (8pp) doi:10.1088/0953-8984/22/15/155801

First-principles study of electronic structures and nonlinear optical properties of $AMoO_3(IO_3)$ (A = Li, Rb and Cs) crystals

Chun-Li Hu and Jiang-Gao Mao[1]

State Key Laboratory of Structural Chemistry, Fujian Institute of Research on the Structure of Matter, Chinese Academy of Sciences, Fuzhou 350002, People's Republic of China

E-mail: mjg@fjirsm.ac.cn

Received 31 January 2010, in final form 2 March 2010
Published 29 March 2010
Online at stacks.iop.org/JPhysCM/22/155801

Abstract

First-principles studies of the geometric structures, electronic structures and second-order nonlinear optical properties of polar alkali metal–Mo(VI)–iodate compounds ($AMoO_3(IO_3)$ (A = Li, Rb and Cs)) have been performed within density functional theory and the independent particle approximation. Our results indicate that, for these compounds, due to the similarity in their anionic groups, the electronic structures and the prominent features of the frequency dependent second-order nonlinear optical susceptibilities are similar, especially for the isostructural Rb and Cs compounds. Also, the calculated SHG coefficients of these compounds are large, which confirms the high response in experimental SHG measurements. By comparing the absolute magnitude of the SHG coefficients, the order $LiMoO_3(IO_3) > RbMoO_3(IO_3) > CsMoO_3(IO_3)$ is clearly established in the low photon energy range. Further analyses based on the spectral and spatial decomposition of the SHG coefficients reveal that the main sources of the SHG properties of these compounds are from the distorted MoO_6 and IO_3^- groups, and can be mainly attributed to the electronic transition from the nonbonding O 2p states (i.e. the lone-pair electrons of O atoms) to the Mo 4d and some I 5p states. It is noticeable that in these compounds, due to the difference in ion size and coordinate environment, the contributions of alkali metals to the SHG processes are very different: for large cations, such as Rb and Cs, they can be neglected, while for the very small Li, they should be included.

(Some figures in this article are in colour only in the electronic version)

1. Introduction

The discovery and development of second-order nonlinear optical (NLO) materials have become a hot research topic in photonic technology in the last two decades [1–3], and depend on the creation of noncentrosymmetric (NCS) structures. Several approaches have been used to obtain NCS structures [4–7]. Among these approaches, the combination of d^0 transition metals (Ti^{4+}, V^{5+}, Nb^{5+}, Mo^{6+}, W^{6+}, etc) and stereoactive lone pairs containing cations (Se(IV), Te(IV), I(V), etc), both of which are susceptible to second-order John–Teller (SOJT) distortion [8, 9], has been proved to be an effective method in creating polar materials with excellent second-order NLO properties due to the 'additive' effects of both types of polarization [10].

On the basis of the above theory, a great number of inorganic second-order NLO crystals have been prepared [11–14]. For example, the recent reported alkali metal–Mo(VI)–iodate compounds ($AMoO_3(IO_3)$, (A = Li, Rb and Cs)) are typical representations of the combination of distorted MoO_6 octahedron and IO_3^- group, and exhibit highly polarized structures [15, 16]. SHG measurements on the powder samples revealed that the response of $LiMoO_3(IO_3)$ is four times that of KDP, and those of the isostructural $RbMoO_3(IO_3)$ and

[1] Author to whom any correspondence should be addressed.

$CsMoO_3(IO_3)$ are about 400 times of α-quartz. Moreover, these compounds are thermally stable (up to 430, 494 and 486 °C, respectively, for Li, Rb and Cs compounds) and show wide transparency regions (1.1–2.8 eV for $LiMoO_3(IO_3)$, and 1–3 eV for Rb and Cs compounds). Hence they are potentially new second-order NLO materials.

Obviously, $LiMoO_3(IO_3)$, $RbMoO_3(IO_3)$ and $CsMoO_3(IO_3)$ have the same chemical formula, and their structures all contain severely distorted MoO_6 octahedra and IO_3^- groups, but what leads to the difference in their SHG response signals? In addition, what are the major sources of SHG properties for these compounds? Does the alkali metal cation contribute to the SHG response? Interpreting these confusing questions in the light of the crystal structures and electronic properties would help us better understand the mechanism of SHG response for this type of NLO material and further shed some light on the design of new excellent nonlinear optical crystals.

Inspired by this, in this paper, we systematically perform theoretical studies on the geometric structures, electronic structures and second-order nonlinear optical properties of $AMoO_3(IO_3)$ (A = Li, Rb and Cs). Our main goal is to find out the crystal structural and electronic structural origins of the high SHG response for these crystals.

2. Computational theory and method

2.1. Electronic structures

The electronic structures calculations are performed using a plane-wave basis set and pseudo-potentials within density functional theory (DFT) implemented in the total-energy code CASTEP [17, 18]. The exchange and correlation effects are treated by Perdew–Burke–Ernzerhof (PBE) in the generalized gradient approximation (GGA) [19]. The interactions between the ionic cores and the electrons are described by the norm-conserving pseudo-potential [20]. The following orbital electrons are treated as valence electrons: Li $2s^1$, Rb $4s^2 4p^6 5s^1$, Cs $5s^2 5p^6 6s^1$, Mo $4d^5 5s^1$, I $5s^2 5p^5$, and O $2s^2 2p^4$. The number of plane waves included in the basis are determined by a cutoff energy of 500 eV, and the numerical integration of the Brillouin zone is performed using a $5 \times 5 \times 3$ Monkhorst–Pack k-point sampling for $LiMoO_3(IO_3)$ and $3 \times 2 \times 3$ for $RbMoO_3(IO_3)$ and $CsMoO_3(IO_3)$.

2.2. Second-order optical susceptibilities

Computational methods on the second-order optical susceptibilities of crystals have been extensively developed in the last few decades [21]. Early in 1963, Butcher and McLean presented a formalism to calculate SHG coefficients based on band structure, although there were some difficulties in dealing with the explicit divergence of their formula [22]. After Aspnes gave a formalism free of divergence in cubic crystals [23], Ghahramani, Moss, and Sipe took another important step in presenting a general approach to avoid the divergence by a new sum rule [24]. Recently, Duan *et al* explored an evaluation technique to reduce the number of k points needed for convergence for the formula given by Ghahramani *et al* ([24]) [25]. To be more specific, Duan *et al*'s formula is easily related to the underlying electronic states, and the contribution of the electronic subsystem to $\chi^{(2)}$ can be analysed based on the spectral and spatial decomposition formula presented by them [25].

So here, the nonlinear optical properties of crystals are calculated using Duan *et al*'s method, which is based on the electronic band structures and optical momentum matrix elements within the independent particle approximation scheme [25]. The imaginary parts of the frequency dependent second-order susceptibilities ($\chi''^{(2)}(2\omega, \omega, \omega)$) are calculated according to the expressions in previous studies [25–27]. Then by using the Kramers–Kronig relations, as required by causality, the real parts are obtained:

$$\chi'^{(2)}(-2\omega, \omega, \omega) = \frac{2}{\pi} P \int_0^\infty \mathrm{d}\omega' \frac{\omega' \chi''^{(2)}(2\omega', \omega', \omega')}{\omega'^2 - \omega^2}. \quad (1)$$

In the present calculations, the δ function in the expressions for $\chi^{(2)}(2\omega, \omega, \omega)$ [25–27] is approximated by a Gaussian function with $\Gamma = 0.2$ eV. Furthermore, to ensure that the real part calculated via Kramer–Kronig transformation (equation (1)) is reliable, more than 300 empty bands are used in the optical calculations.

Although the DFT–GGA gives a rather good wavefunction, it fails to correctly predict the CB energies. So the CB energy should be corrected by adding a scissor operator, meanwhile, the momentum matrix elements should also be renormalized according to [25, 28]

$$P_{ij} = P_{ij}^{\mathrm{GGA}} \left[1 + \frac{\Delta(\delta_{ic} - \delta_{jc})}{\omega_{ij}^{\mathrm{GGA}}} \right], \quad (2)$$

where Δ is the scissor operator, which is chosen to shift the band-gap to the experimental value of the crystal. The Kronecker symbol δ_{ic} assumes the value unity only when state i belongs to the CB.

To identify the contribution of non-equivalent atoms or electronic states to the SHG response in these crystals, we perform the spectral and spatial decomposition according to previous studies [25, 28]. The $\chi^{(2)}$ components at 1064 nm are decomposed into contributions from a set of non-overlapping volumes $\{\Omega_n\}$ (which cover the whole unit cell), and the contributions from an energy interval of either the VB states (i) or the CB states (j) are defined as

$$\chi^{(2)}(\Omega_n, E_v) = \int_{\mathrm{BZ}} \frac{\mathrm{d}k}{4\pi^3} \sum_{i \in \mathrm{VB}} \sum_{j \in \mathrm{CB}} \sum_l \chi^{ijl} \delta(E_i - E_v) \times \left\{ \frac{\Omega}{\Omega_n} \langle i/i \rangle_{\Omega_n} \right\} \quad (3)$$

and

$$\chi^{(2)}(\Omega_n, E_c) = \int_{\mathrm{BZ}} \frac{\mathrm{d}k}{4\pi^3} \sum_{i \in \mathrm{VB}} \sum_{j \in \mathrm{CB}} \sum_l \chi^{ijl} \delta(E_j - E_c) \times \left\{ \frac{\Omega}{\Omega_n} \langle j/j \rangle_{\Omega_n} \right\}. \quad (4)$$

They can be understood as the (volume-normalized) average density of the NLO contribution from region Ω_n at the corresponding energy E_v or E_c.

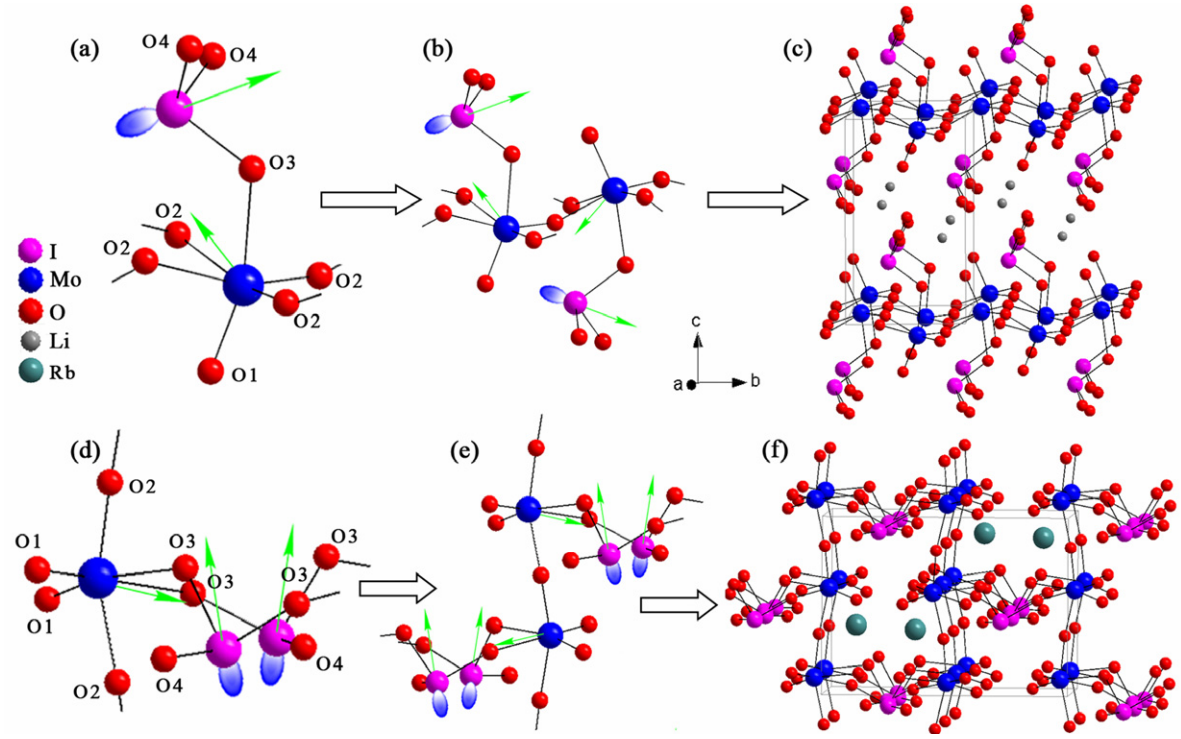

Figure 1. The structural building units and the whole structures of $LiMoO_3(IO_3)$ ((a)–(c)) and $RbMoO_3(IO_3)$ ((d)–(f)). The green arrows point to the directions of local dipole moments.

All of the optical properties and dipole moments calculations of these compounds in this paper are based on their principal dielectric axis coordinate systems[2].

3. Results and discussion

3.1. Geometric and electronic structures

For the purpose of discussion, the structural building units and the whole structures of $LiMoO_3(IO_3)$ and $RbMoO_3(IO_3)$ are illustrated in figure 1. $LiMoO_3(IO_3)$ crystallizes in acentric space group $P2_1$ (No. 4), and features a 2D structure containing $[MoO_3(IO_3)]^-$ anionic layers separated by Li^+ counterions (figure 1(c)). In the layer configuration of $LiMoO_3(IO_3)$ (figures 1(a) and (b)), each MoO_6 octahedron shares four in-plane vertices with similar adjacent units to form a WO_3-like layer, and half of the apical oxygen atoms of the MoO_6 octahedra are capped by IO_3^- groups, that are alternately situated on both sides of the infinite Mo–O layers due to the existence of the 2_1 screw axis in the b direction [15]. Both Rb and Cs compounds crystallize in acentric space group $Pna2_1$ (No. 33) and feature 3D networks composed of 1D molybdenum oxide chains that are bridged by IO_3^- groups, forming 1D tunnels filled by Rb^+ or Cs^+ cations (figure 1(f)). In the anionic structures of the Rb and Cs compounds (figures 1(d) and (e)), MoO_6 octahedra share corners with neighbouring octahedra to form 1D chains, in which MoO_2^{2+} alternate their orientation in chain translation. The bridging IO_3^- groups between the chains are situated on all sides of the chains and connect them together to create a 3D polar network [16]. It is noticeable that in these compounds, the alkali metal cations are located in different coordinate environments: the smaller Li^+ ion is in a tetrahedral LiO_4 geometry, while the larger Rb^+ and Cs^+ cations are surrounded by nine to ten O atoms.

The calculated band structures are plotted in figure 2 and the band gaps are listed in table 1. For $LiMoO_3(IO_3)$ (figure 2(a)), the highest point of the valence band (VB) is situated at the Z point, and the lowest point of the conduction band (CB) is at the G point, so it is an indirect band-gap compound. $RbMoO_3(IO_3)$ and $CsMoO_3(IO_3)$ are isostructural and their band dispersions behave very similarly, so only the band structure of $RbMoO_3(IO_3)$ is displayed. It is obvious that they are direct band-gap crystals (from G to G) (figure 2(b)). The calculated band gaps of $LiMoO_3(IO_3)$, $RbMoO_3(IO_3)$ and $CsMoO_3(IO_3)$ are 2.30, 2.23 and 2.34 eV, respectively, much smaller than the experimental values of 2.80, 3.10 and 3.10 eV. This is not surprising, because it is well known that the DFT–GGA does not accurately describe the eigenvalues of the electronic states, causing quantitative underestimation of band gaps [29, 30].

The bands can be assigned according to the total and partial density of states (TDOS and PDOS, see figure 3). For the Li compound (figure 3(a)), the bottommost VB region, ranging from −20 to −18.5 eV, is composed of O 2s and I 5s states. The bands between −17.5 and −15 eV mainly originate from O 2s states mixed with small amounts of I 5p and

[2] For the method of the principal dielectric axis determination for the monoclinic $LiMoO_3(IO_3)$ crystal, see [13, 14]. The rotation angle θ between the original coordinate axes and the principal dielectric axes in the a–c plane was calculated to be 6.7067°.

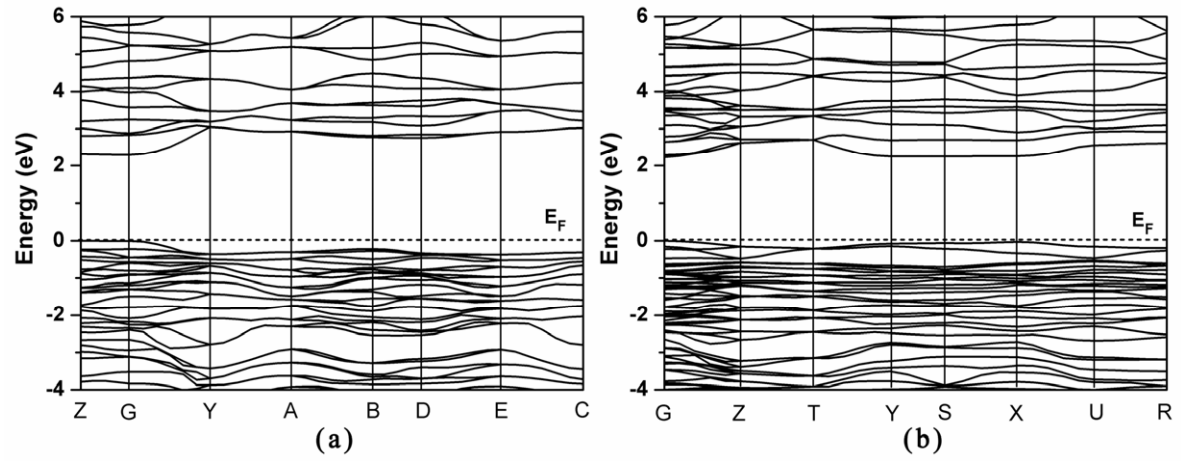

Figure 2. Calculated band structures of $LiMoO_3(IO_3)$ (a) and $RbMoO_3(IO_3)$ (b).

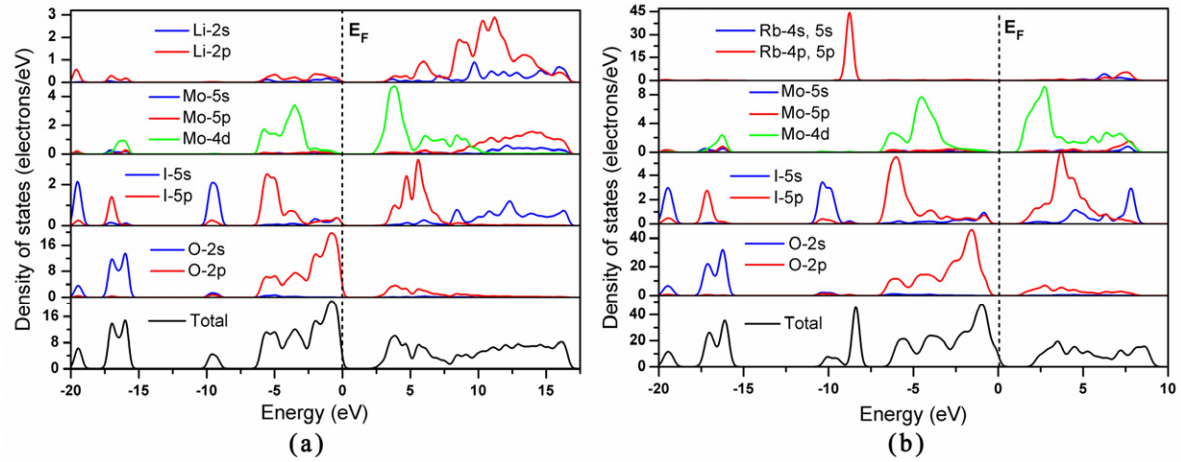

Figure 3. Total and partial density of states of $LiMoO_3(IO_3)$ (a) and $RbMoO_3(IO_3)$ (b).

Table 1. The calculated band gaps (E_g), scissor (ΔE_g), $\chi^{(2)}$, dipole moment and the contributions of groups to $\chi^{(2)}$ of the $AMoO_3(IO_3)$ (A = Li, Rb and Cs) compounds.

	$LiMoO_3(IO_3)$	$RbMoO_3(IO_3)$	$CsMoO_3(IO_3)$
E_g^a (eV)	2.30 (2.80[b])	2.23 (3.10[c])	2.34 (3.10[c])
ΔE_g (eV)	0.50	0.87	0.76
$\chi^{(2)}$ [d] ($\times 10^{-8}$ esu)	$\chi^{(2)}_{112} = -6.70\ (-4.58)$	$\chi^{(2)}_{113} = -1.20\ (-0.81)$	$\chi^{(2)}_{113} = -0.52\ (-0.21)$
	$\chi^{(2)}_{123} = 1.02\ (0.92)$	$\chi^{(2)}_{223} = -0.13\ (-0.22)$	$\chi^{(2)}_{223} = -1.12\ (-0.70)$
	$\chi^{(2)}_{222} = 1.01\ (0.62)$	$\chi^{(2)}_{333} = -5.66\ (-3.24)$	$\chi^{(2)}_{333} = -4.56\ (-2.80)$
	$\chi^{(2)}_{323} = 1.17\ (1.20)$		
Local dipole moment (D)	$MoO_6 = 9.20$	$MoO_6 = 11.79$	$MoO_6 = 11.75$
	$IO_3 = 5.21$	$IO_3 = 5.89$	$IO_3 = 5.73$
	$LiO_4 = 6.50$		
Net dipole moment in unit volume (D Å^{-3})	3.69×10^{-2} (along b axis)	2.81×10^{-2} (along c axis)	2.06×10^{-2} (along c axis)
Contributions to $\chi^{(2)}$ (%)	$MoO_6 = 58.47$	$MoO_6 = 79.30$	$MoO_6 = 78.39$
	$IO_3 = 35.82$	$IO_3 = 19.73$	$IO_3 = 20.57$
	$Li^+ = 5.71$	$Rb^+ = 0.97$	$Cs^+ = 1.04$

[a] The calculated band gaps and the experimental gaps (in brackets).
[b] Reference [15]. [c] Reference [16].
[d] The calculated $\chi^{(2)}$ at 1064 nm and the corresponding $\chi^{(2)}(0)$ (in brackets), the $\chi^{(2)}(0)$ are calculated by adopting Lin's formula.

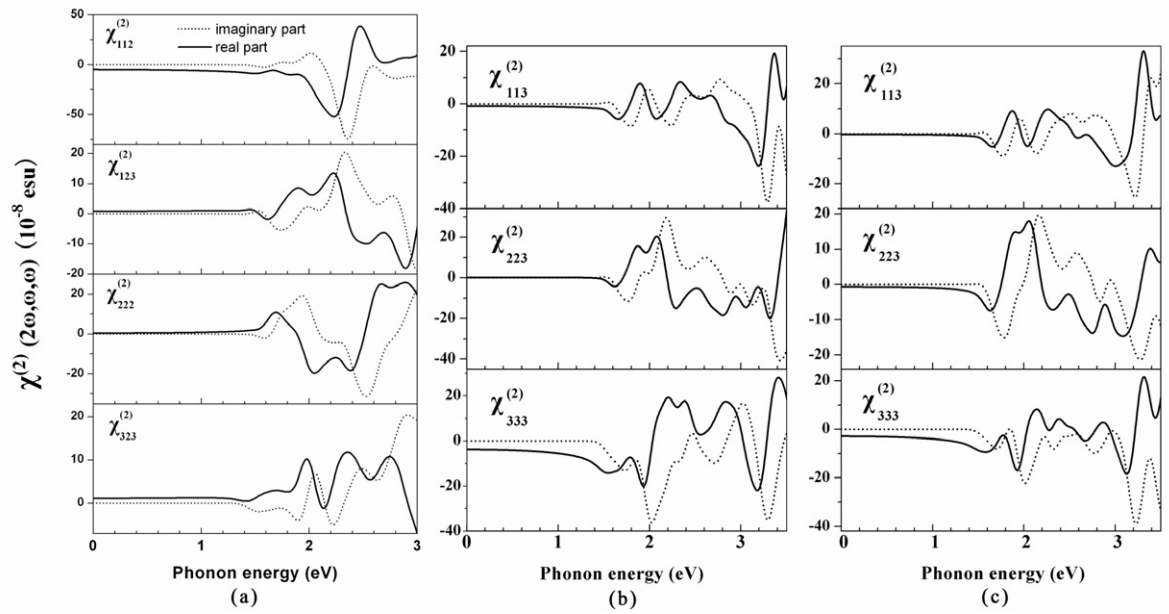

Figure 4. Calculated real and imaginary parts of $\chi^{(2)}(2\omega, \omega, \omega)$ of $LiMoO_3(IO_3)$ (a), $RbMoO_3(IO_3)$ (b) and $CsMoO_3(IO_3)$ (c).

Mo 4d states. I 5s states dominate the energy region −10.5–(−8.7) eV. We will focus on the highest VB and the lowest CB, which account for most of the bonding character in the compounds. The highest VB (−6.3–0 eV) can be divided into two energy regions. Between −6.3 and −2.5 eV, O 2p states overlap fully with Mo 4d and I 5p, indicating well-defined p–d hybridizations of MoO_6 octahedron and I–O covalent interactions. The VB in the vicinity of E_F (−2.5–0 eV) mainly comes from O 2p, which belongs to the nonbonding states, i.e. the lone-pair electrons states of O 2p. The CB can also be divided into two regions. The lowest CB (<7.5 eV) originates mainly from the contribution of the localized Mo 4d, I 5p and O 2p states. In the region far from E_F (7.5–17 eV), the DOS is largely dispersive. Li 2p plays an important role in the region, followed by the Mo 5p, I 5s and Li 2s states.

Since Rb and Cs compounds are isostructural, their DOSs behave nearly the same. Here, as a representation, only the DOS of $RbMoO_3(IO_3)$ is displayed (figure 3(b)). It is clear that the PDOS of the anionic group $[MoO_3(IO_3)]^-$ in the Rb (or Cs) compound behaves very similarly to that in the Li compound, which may be caused by the similar bonding manner in these crystals. The significant difference between Li and Rb (or Cs) compounds comes from the cation states: Li^+ exhibits a dispersive character and overlaps with O states in VB and CB, while the states of Rb^+ (or Cs^+) are concentrated in some narrow energy regions, e.g. a very high peak of Rb 4p locates at −7.9–(−8.9) eV of VB. This reveals some covalent character of Li–O bonds in LiO_4 and the pure ionicity of Rb–O (or Cs–O) bonds.

3.2. Second-order optical susceptibilities

On the basis of the space groups and the Kleinman symmetry, $LiMoO_3(IO_3)$, $RbMoO_3(IO_3)$ and $CsMoO_3(IO_3)$ have four, three and three non-vanishing independent $\chi^{(2)}$ components, respectively. We display the imaginary and real parts of the frequency dependent second-order optical susceptibilities $[\chi^{(2)}(2\omega, \omega, \omega)]$ of $LiMoO_3(IO_3)$, $RbMoO_3(IO_3)$ and $CsMoO_3(IO_3)$ in figure 4. From these figures, it is found that the prominent features in these $\chi^{(2)}$ curves behave similarly. We take the Rb compound as the example to describe the $\chi^{(2)}$ curves in detail. The real parts of all $\chi^{(2)}$ components of $RbMoO_3(IO_3)$ remain nearly constant at low photon energy up to ∼0.5 eV, and increase gradually in magnitude as the photon energy increases and peak at the absorption edge of ∼1.5 eV, then descend and become positive and form multiple peaks. Later they become negative again and form the highest peak in the vicinity of the gap energy of ∼3.1 eV. Beyond ∼3.1 eV, the curves oscillate sharply and gradually diminish as the photon energy further increases. The imaginary (absorptive) parts of $\chi^{(2)}$ in $RbMoO_3(IO_3)$ are zero when the photon energy is lower than ∼1.5 eV ($\approx E_g/2$), and there is an intense oscillation between 1.5 and 3.5 eV, with several obvious peaks. A detailed analysis indicates that the peaks around $E_g/2$ are due to the double photon resonances, while in contrast, those around E_g come from the single photon resonances. Similar analyses of $\chi^{(2)}(2\omega, \omega, \omega)$ can also be performed on the other two compounds and, particularly for the Cs compound, the line shape of the $\chi^{(2)}$ curves are nearly the same as the corresponding components of the isostructural $RbMoO_3(IO_3)$.

The experimental measurements on the powder samples revealed that the SHG response at 1064 nm is about four times that of KDP for $LiMoO_3(IO_3)$, and about 400 times that of α-quartz for the Rb and Cs compounds [15, 16]. However, due to the inaccurate and semi-quantitative character of the powder sample SHG measurements, adding the different reference samples, i.e. α-quartz or KDP, direct comparison of the SHG intensity for these compounds is unavailable. Here, by comparing the absolute magnitude

of the highest $\chi^{(2)}$ components of these compounds at 1064 nm (see table 1), the order $LiMoO_3(IO_3)$ ($\chi^{(2)}_{112}$ = 6.70 × 10^{-8} esu) > $RbMoO_3(IO_3)$ ($\chi^{(2)}_{333}$ = 5.66 × 10^{-8} esu) > $CsMoO_3(IO_3)$ ($\chi^{(2)}_{333}$ = 4.56 × 10^{-8} esu) is clearly found. (In fact, the above order exists in the low energy range of 0–1.4 eV.) It is noticeable that Duan's SHG formula does not accurately bear the Kleinman symmetry [28]. To test the reliability of the above results, we also adopt Lin's method [31], which explicitly shows Kleinman symmetry but could only give a static value, to calculate $\chi^{(2)}(0)$ of these compounds. The results repeat the above order $LiMoO_3(IO_3)$ [$\chi^{(2)}_{112}(0)$ = 4.58 × 10^{-8} esu] > $RbMoO_3(IO_3)$ [$\chi^{(2)}_{333}(0)$ = 3.24 × 10^{-8} esu] > $CsMoO_3(IO_3)$ [$\chi^{(2)}_{333}(0)$ = 2.80 × 10^{-8} esu] for their highest components (see table 1).

3.3. Geometric and electronic structure origins of the SHG response

In this section, we attempt to explore the sources of the high SHG response of these compounds in the light of the geometric structures and electronic properties.

It is well known that the SHG response is greatly related to the polarity magnitude of the crystal, which is determined by the local dipole moment of each polar group and its geometric arrangement. The local dipole moments of polar groups in these crystals are calculated according to previous studies [32, 33]. Obviously, in these compounds, both Mo^{6+} and I^{5+} cations are in an asymmetric coordination environment. In $LiMoO_3(IO_3)$, the Mo^{6+} cation exhibits an intra-octahedral distortion towards a face of the MoO_6 octahedron (a C_3 distortion) [15], resulting in a local dipole moment of 9.20 D (see figure 1(a) and table 1). In Rb and Cs compounds, the Mo^{6+} cation has a C_2 distortion [16], and the local dipole moments are 11.79 and 11.75 D, respectively (see figure 1(d) and table 1). The I^{5+} cations in these compounds are in distorted trigonal–pyramidal environments, and the local dipole moments of IO_3^- are calculated to be 5.21, 5.89 and 5.73 D in the Li, Rb and Cs compounds, respectively (see table 1). As stated above, due to large difference in their radii, the alkali metal counterions in these compounds are located in different coordinate environments and exhibit different bonding properties with the surrounding O. The large Rb^+ or Cs^+ cations are surrounded by nine to ten oxygen atoms and exhibit pure ionicity, while the very small Li^+ is in a low-coordinated LiO_4 tetrahedron and the Li–O bonds have some covalent character. This can be clearly seen from the above electronic structure analyses. So, the local dipole moment of the distorted LiO_4 tetrahedron in $LiMoO_3(IO_3)$ should also be included, that is 6.50 D. The local dipole moments of these asymmetric groups provide an essential condition for the high SHG response of these compounds, but it may not the sole cause. Due to the symmetry restriction of the crystals, the polarization directions of the distorted groups are opposite along some coordinate axes and the dipole moments just cancel out. This is confirmed by our calculated results, that in the a and c directions for $LiMoO_3(IO_3)$ as well as the a and b directions for $RbMoO_3(IO_3)$ and $CsMoO_3(IO_3)$,

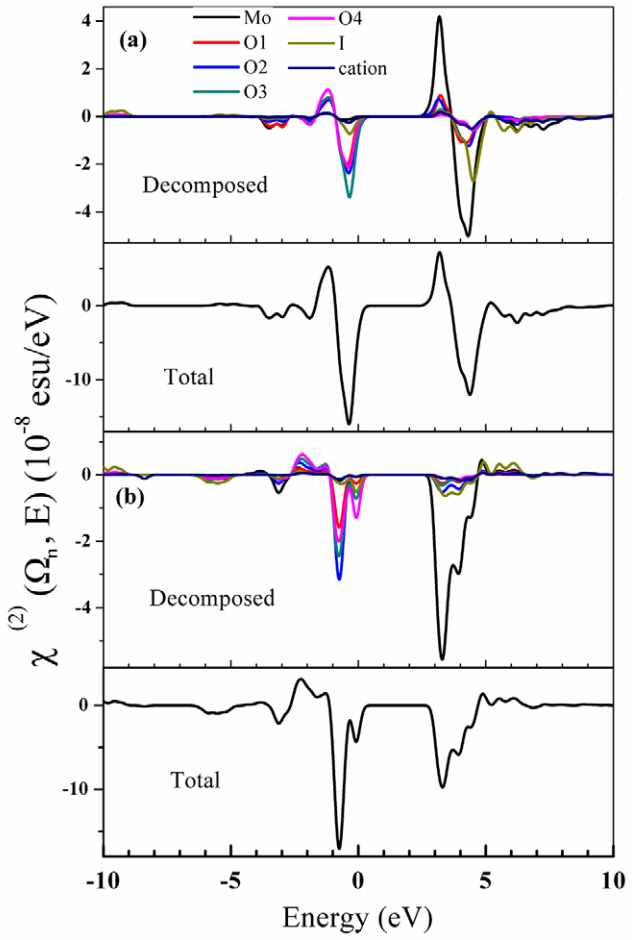

Figure 5. Spectral and spatial decomposition of $\chi^{(2)}_{112}$ for $LiMoO_3(IO_3)$ (a) and $\chi^{(2)}_{333}$ for $RbMoO_3(IO_3)$ (b) at 1064 nm. The non-equivalent atoms (Mo, O1, O2, O3, O4 and I) are marked in figure 1.

the dipole moments are zero, and only the dipole moments along the b direction for Li and the c direction for Rb and Cs compounds are left (see figure 1). The results also indicate that there is the order $LiMoO_3(IO_3)$ (along b axis, 3.69 × 10^{-2} D Å^{-3}) > $RbMoO_3(IO_3)$ (along c axis, 2.81 × 10^{-2} D Å^{-3}) > $CsMoO_3(IO_3)$ (along c axis, 2.06 × 10^{-2} D Å^{-3}) for the net dipole moments in a unit volume (see table 1). This is in agreement with the order of the SHG magnitude for these compounds.

Also, the macroscopic SHG response of the material can be the summation of the contributions of all polar groups. Different groups and different atoms in the same group must play different roles in the NLO process. Hence, it is crucial to identify the role played by each atom or group in one unit cell. In addition, it is also very important to make clear the relationship between the SHG coefficients and the electronic structures of the compounds. So, here, we perform the spectral and spatial decomposition of the SHG coefficients at 1064 nm, to show clearly how much each group of electron states and each constituent of the crystals contribute. For brevity, only the highest components of the compounds are studied, and the decomposition pictures are displayed in figure 5.

The $\chi^{(2)}_{112}$ of $LiMoO_3(IO_3)$ has a negative value at 1064 nm. The main contributions to $\chi^{(2)}_{112}$ are localized in the energy ranges of −0.9–0 eV in the VB and 3.7–5.0 eV in the CB, while the regions of −1.7–(−0.9) eV in the VB and 2.6–3.7 eV in the CB give smaller but opposite contributions to $\chi^{(2)}_{112}$ (see the 'total' panel in figure 5(a)). From the 'decomposed' panel of figure 5(a), it is obvious that the main structure of curve 'total' in the VB is contributed by that of O atoms, whose peaks are noticeably greater than other atoms. But not all the O 2p states that extend from −6.3 eV to the VB top have the same contribution, only the upper part (−1.7–0 eV) contributes significantly, which consists of the nonbonding 2p molecular orbitals. It is also shown that the contributions of Mo and I to $\chi^{(2)}_{112}$ in the VB come to nearly zero and are negligible, though the PDOSs of Mo and I in the VB are not small (see figure 3). An entirely different picture is shown with respect to the CB. The role of the Mo and I atoms become significant in the CB. The main contributed region from 2.6 to 5.0 eV in the CB originates mostly from Mo, the next largest is I. In this region, O atoms also have obvious contributions, and the peak shapes are similar to Mo and I, indicating the strong interactions between them. It is necessary to note that the Li^+ cation still has a small contribution dispersed in the range of 2.6–5.0 eV, where the main contributions of O atoms concentrate. This reveals that Li has weak interactions to its neighbour O atoms.

The decomposition curves of the corresponding SHG components of $CsMoO_3(IO_3)$ behave nearly the same as $RbMoO_3(IO_3)$, so only $RbMoO_3(IO_3)$ is displayed, as shown in figure 5(b). Similar to $LiMoO_3(IO_3)$, the decomposition pictures of $\chi^{(2)}_{333}$ of Rb and Cs compounds also show that the VB is dominated by the nonbonding O 2p states and the CB is contributed to by Mo 4d mixing with some I 5p states. Hence, it is concluded that the SHG properties of these compounds can be mainly attributed to the interband electronic transition from the nonbonding O 2p states (i.e. the lone-pair electrons of O atoms) to the Mo 4d and some I 5p states. Further, we also carry out the integral calculations for the decomposition curves over the VB or the CB, to define the contribution percentage to $\chi^{(2)}$ of each atom and group (see table 1). The results show that the main contributions to $\chi^{(2)}$ in these compounds are from the distorted MoO_6 and IO_3^- groups, i.e. the anionic group; and the contribution percentages of Rb^+ and Cs^+ cations (about 0.97 and 1.04, respectively) are much smaller than that of Li^+ in its compound (about 5.71). It is clear that in these compounds, due to the difference in ion size and coordinate environment, the contributions of alkali metals to the SHG processes can be very different: for large cations, such as Rb and Cs, they can be neglected, while for the very small Li, they should be included.

4. Conclusion

We have systematically studied the geometric structures, electronic properties and second-order NLO properties of three polar crystals, $LiMoO_3(IO_3)$, $RbMoO_3(IO_3)$ and $CsMoO_3(IO_3)$ employing the DFT–GGA method and the independent particle approximation. Further, by calculating the dipole moments and performing the spectral and spatial decomposition of $\chi^{(2)}$ at 1064 nm, we attempt to explore the crystal structural and electronic structural origins of the high SHG response of these second-order NLO crystals.

The results show that the second-order optical susceptibilities of these compounds are large, which confirms their high SHG response in experimental measurements. These compounds all contain the same building groups: the distorted MoO_6 octahedron and IO_3^- group. This causes many similarities in their electronic properties, e.g. the similar band gaps and band components near the band-gap region. Also, the prominent features in frequency dependent second-order susceptibilities of these crystals are similar, especially for the isostructural $RbMoO_3(IO_3)$ and $CsMoO_3(IO_3)$. Meanwhile, the geometric arrangement of the building groups in these compounds brings a difference in their polarity magnitudes, and hence the second-order NLO susceptibilities: the order Li > Rb > Cs is obtained for both net dipole moments and SHG coefficients. Further analyses, based on the spectral and spatial decomposition of $\chi^{(2)}$, reveal that the main sources of the high SHG response of these compounds are from the distorted MoO_6 and IO_3^- groups, and can be mainly attributed to the interband electronic transition from the nonbonding O 2p states (i.e. the lone-pair electrons of O atoms) to the Mo 4d and some I 5p states. It is noticeable that in these compounds, due to the difference in ion size and coordinate environment, the contributions of alkali metals to the SHG processes are very different: for large cations, such as Rb and Cs, they can be neglected, while for the very small Li, they should be included.

Acknowledgments

We thank the National Natural Science Foundation of China (Nos 20825104, 20731006 and 20821061) for financial support.

References

[1] Chen C and Liu G 1986 *Annu. Rev. Mater. Sci.* **16** 203
[2] Ok K M and Halasyamani P S 2006 *Chem. Soc. Rev.* **35** 710
[3] Wickleder M S 2002 *Chem. Rev.* **102** 2011
[4] Holman K T, Pivovar A M and Ward M D 2001 *Science* **294** 1907
[5] Lin W, Evans O R, Xiong R G and Wang Z 1998 *J. Am. Chem. Soc.* **120** 13272
[6] Porter Y, Ok K M, Bhuvanesh N S P and Halasyamani P S 2001 *Chem. Mater.* **13** 1910
[7] Norquist A J, Heier K R, Halasyamani P S, Stern C L and Poeppelmeier K R 2001 *Inorg. Chem.* **40** 2015
[8] Pearson R G 1969 *J. Am. Chem. Soc.* **91** 4947
[9] Wheeler R A, Whangbo M H, Hughbanks T, Hoffmann R, Burdett J K and Albright T A 1986 *J. Am. Chem. Soc.* **108** 2222
[10] Halasyamani P S 2004 *Chem. Mater.* **16** 3586
[11] Ra H S, Ok K M and Halasyamani P S 2003 *J. Am. Chem. Soc.* **125** 7764
[12] Chi E O, Ok K M, Porter Y and Halasyamani P S 2006 *Chem. Mater.* **18** 2070
[13] Yang B P, Hu C L, Xu X, Sun C F, Zhang J H and Mao J G 2010 *Chem. Mater.* **22** 1545

[14] Sun C F, Hu C L, Xu X, Ling J B, Hu T, Kong F, Long X F and Mao J G 2009 *J. Am. Chem. Soc.* **131** 9486
[15] Chen X, Zhang L, Chang X, Xue H, Zang H, Xiao W, Song X and Yan H 2007 *J. Alloys Compounds* **428** 54
[16] Sykora R E, Ok K M, Halasyamani P S and Albrecht-Schmitt T E 2002 *J. Am. Chem. Soc.* **124** 1951
[17] Milman V, Winkler B, White J A, Pickard C J, Payne M C, Akhmatskaya E V and Nobes R H 2000 *Int. J. Quantum Chem.* **77** 895
[18] Segall M D, Lindan P L D, Probert M J, Pickard C J, Hasnip P J, Clark S J and Payne M C 2002 *J. Phys.: Condens. Matter* **14** 2717
[19] Perdew J P, Burke K and Ernzerhof M 1996 *Phys. Rev. Lett.* **77** 3865
[20] Lin J S, Qteish A, Payne M C and Heine V 1993 *Phys. Rev.* B **47** 4174
[21] Champagne B and Bishop D M 2003 *Adv. Chem. Phys.* **126** 41
[22] Butcher P N and McLean T P 1963 *Proc. Phys. Soc. Lond.* **81** 219
[23] Aspnes D E 1972 *Phys. Rev.* B **6** 4648
[24] Ghahramani E, Moss D J and Sipe J E 1991 *Phys. Rev.* B **43** 8990
[25] Duan C G, Li J, Gu Z Q and Wang D S 1999 *Phys. Rev.* B **60** 9435
[26] Guo G Y, Chu K C, Wang D S and Duan C G 2004 *Phys. Rev.* B **69** 205416
[27] Guo G Y and Lin J C 2005 *Phys. Rev.* B **72** 075416
[28] Duan C G, Li J, Gu Z Q and Wang D S 1999 *Phys. Rev.* B **59** 369
[29] Okoye C M I 2003 *J. Phys.: Condens. Matter* **15** 5945
[30] Huang S P, Cheng W D, Wu D S, Li X D, Lan Y Z, Li F F, Shen J, Zhang H and Gong Y J 2006 *J. Appl. Phys.* **99** 013516
[31] Lin J, Lee M H, Liu Z P, Chen C and Pickard C J 1999 *Phys. Rev.* B **60** 13380
[32] Maggard P A, Nault T S, Stern C L and Poeppelmeier K R 2003 *J. Solid State Chem.* **175** 27
[33] Izumi H K, Kirsch J E, Stern C L and Poeppelmeier K R 2005 *Inorg. Chem.* **44** 884